RSC Advances

ROYAL SOCIETY OF CHEMISTRY

www.rsc.org/advances

Multi-level structure bio-carbon composite with polyaniline for high performance supercapacitor

Guofu Ma[a*]; Haiping Wang[a]; Kanjun Sun[b]; Hui Peng[a]; Yajuan Wu[a]; Ziqiang Lei[a*]

[a]*Key Laboratory of Eco-Environment-Related Polymer Materials of Ministry of Education, Key Laboratory of Polymer Materials of Gansu Province, College of Chemistry and Chemical Engineering, Northwest Normal University, Lanzhou 730070, P.R. China*

[b]*College of Chemistry and Environmental Science, Lanzhou City University Lanzhou 730070, P.R. China.*

E-mail: magf@nwnu.edu.cn, leizq@nwnu.edu.cn

ABSTRACT

A novel activated carbon material with multi-level structure is prepared by KOH-activation of chestnut shell at 800 ^{o}C (CAC8). The specific surface area and pore volume of the activated carbon obtained are as high as 1568.0 m^2 g^{-1} and 0.94 cm^3 g^{-1}. The electrochemical performances of the CAC8 are very promising, the specific capacitance is 207 F g^{-1} at current density of 1 A g^{-1} in 1 M H_2SO_4 electrolyte. The CAC8/PANI composite was synthesized through an interfacial polymerization method, which presents good electrochemical performance, including an excellent specific capacitance of 597 F g^{-1} and 80% retention of capacitance after 1000 cycles at a current density of 1 A g^{-1} in 1 M H_2SO_4 electrolyte. The high electrochemistry performance can be due to the use of the multi-level structure carbon that improve charge transfer performance of CAC8/PANI composite materials.

* Corresponding author Tel.: +86 931 7975121; fax: +86 931 7975121.
E-mail addresses: magf@nwnu.edu.cn, leizq@nwnu.edu.cn

KEYWORDS: Bio-carbon; Polyaniline; Composite; Supercapacitor

1. Introduction

In the wake of depleting fossil fuel reserve and increasing awareness for pollution control, industry and research centers around the world are searching for viable alternatives to the development of renewable energy production that can compete with all available technologies [1]. In this quest, supercapacitors or electrochemical capacitors represent a unique class of energy storage devices that exhibit high power capability, long cycle lifetime, and fast charge and discharge rates, lower maintenance cost, and environmental friendliness. Such outstanding properties make them promising energy storage devices in a wide range of applications, such as portable electronics, mobile communications, hybrid electric vehicles, memory backup systems, large industrial equipments, and military devices [2-5]. Most researches have focused on the development of different electrode materials such as transition metal oxides, various forms of carbon, and conducting polymers [6-8].

As a typical carbon, activated carbons are the most widely used electrode material for supercapacitors because of their high surface area and relatively good electrical conductivity. Recent years, the use of biomass materials to produce carbon becomes of interest when business costs, wide availability, and energy/environmental concern are considered. These porous carbons are generally produced by the carbonization of the original biomass materials and the further chemical or physical activation. To date, various biomass derived porous carbons, such as from cells [9], membranes [10], cellulose [11], rice hull [12], paper pulp [13] and coconut shells [14],

have been reported. These materials have showed great potential as electrode materials for supercapacitors.

Among conducting polymers, polyaniline (PANI) has long been a very favorable material in various electrical devices due to its ease of synthesis, adjustable conductivity, perfect processability, and special redox activity [15]. However, PANI exhibits poor rate capability, temperature dependence and inferior cycling stability. Previous reports have described that coupling nanostructured PANI to inorganic materials (carbon materials, metal oxides or hydroxides) to prepare a composite to be used in the supercapacitors with an improved conductivity, better cycleability, specific capacitance and mechanical stability [16]. Up to now, coupling nanostructured PANI to carbonaceous materials can improve the utilization of PANI and provide a short transport path for ion and electron [17-22]. For example, Liu et al [23] prepared an amide group-connected graphene-polyaniline nanofiber hybrid, which had a specific capacitance of 579.8 and 361.9 F g^{-1} at current densities of 0.3 and 1 A g^{-1}. Sarker and Hong [24] obtained a graphene/polyaniline bilayer used as the supercapacitor electrode materials yielded a volumetric capacitance of 584 F cm^{-3} at a current density of 3.0 A cm^{-3}. Fan et al [25] fabricated hierarchical nanocomposites of polyaniline nanorods grown on the surface of carbon nanotubes for high performance supercapacitor electrodes. However, these synthetic methods reported still have disadvantages, such as time-consuming, cost effective due to the utilization of expensive raw materials and so on.

The biomass resources for energy storage applications are abundant. Chestnut is

one of the oldest living fossils on the earth and chestnut shell-based activated carbons hybridized with materials (conducting polymers, metal oxides or hydroxides) to prepare composites are rarely reported as the electrode materials for supercapacitors to our knowledge.

In this paper, the chestnut shell was used as the starting material to fabricate chestnut shell based activated carbons (CACs), The CACs/PANI composites were synthesized by interfacial polymerization. Electrochemical tests shows the CAC8/PANI composite electrode has good chemical stability and low electron transfer resistance, which can be attributed to the large specific surface area with unique porous nanocones architectures and the short ion-transport distance.

2. Experimental

2.1. Materials

Chestnut shells were obtained from a local fruit stall and cut into small pieces, dried in sunlight and powdered. Aniline monomer (Shanghai Chemical Works, China) was distilled under reduced pressure, ammonium persulfate (APS, Tianjing Damao Chemical Co., China) were used as received. All solutions were prepared in deionized water. All other chemical reagents were in analytical grade.

2.2. Preparation chestnut shell based activated carbons (CACs) and CACs/PANI composites

The activated carbons were prepared from chestnut shells, which were performed by mixing the dried chestnut shells with KOH solution at an impregnation ratio of 5:2 (mass KOH: mass chestnut shells) and stirring at 60 ^{o}C for 3 h. The resulting slurry

was dried in an oven for at least 24 h at 100 ^{o}C. The dried sample was carbonized between 500 and 900 ^{o}C with temperature ramp rate of 5 ^{o}C min^{-1} and kept for 2.5 h under flowing nitrogen atmosphere in a tubular furnace. The final product was washed repeatedly with 0.5 M HCl until the pH of the washing solution reach 6.5 and then washed with distilled water, filtered, dried and the biomass carbons were labeled as CAC5, CAC6, CAC7, CAC8 and CAC9 according the carbonized temperature.

The CACs/PANI composites were synthesized by an interfacial polymerization method. The typical procedure was as follows: CACs (0.03 g) was added into a mixed solution of 50 mL of isopropyl alcohol and 50 mL of 1 M H_2SO_4, and the mixture was sonicated for 30 min to obtain a well-dispersed suspension. Then ammonium persulfate (APS, 0.76 g) was dissolved in the above solution to form a water phase. Aniline monomes (0.50 g) was dissolved in 100 mL of dichloromethane to form an oil phase. The water and oil phases were then carefully transferred to a 500 mL beaker. The reaction was performed at 0 °C for 24 h, then the resulting product was filtered, washed with deionized water and ethanol several times, dried at 60 °C under a vacuum to obtain the CACs/PANI composites (about 0.4 g). The materials obtained were referred to as CAC5/PANI, CAC6/PANI, CAC7/PANI, CAC8/PANI and CAC9/PANI. For comparison, pure PANI was synthesized through a procedure similar to that above without the presence of CAC. According the mass of CACs we have used and the CACs/PANI composites we obtained, the PANI mass percent content in the composite is about 92.5 % using the following equation:

$$wt_{PANI}(\%) = (m_{CACs/PANI} - m_{CAC})/m_{CACs/PANI} \times 100$$

2.3. Characterizations

The morphology and structure of the pure PANI, CAC8 and CACs/PANI

composites were examined with field emission scanning electron microscopy (FESEM, JSM-6701F, Japan) at an accelerating voltage of 5.0 kV, and transmission electron microscopy (TEM, JEM-2010 Japan). X-ray diffraction (XRD) of samples was performed on a diffractometer (D/Max-2400, Rigaku) using Cu Kα radiation (k =1.5418 Å) at 40 kV, 100 mA. The 2θ range used in the measurements was from 5 to 80°. The Brunauer-Emmett-Teller (BET) surface area (SBET) of the powders was analyzed by nitrogen adsorption in a Micromeritics ASAP 2020 nitrogen adsorption apparatus (U.S.A.).

2.4. Electrochemical measurements

A typical three-electrode test cells was used for electrochemical measurement on the electrochemical working station (CHI660D, Chenghua, Shanghai China). All the measurements were carried out in 1 M H_2SO_4 electrolyte at room temperature. The glassy carbon electrode with a diameter of 3 mm was used as the working electrode. Platinum electrode served as the counter electrode and saturated calomel electrode (SCE) as the reference electrode.

The fabrication of the working electrodes refers to Ref. [26]. Typically, 4 mg of CACs/PANI was ultrasonically dispersed in 400 μL of deionized water, and 4 μL of the polytetrafluoroethylene (PTFE) emulsion (60 wt%) was added to this dispersion. 2 μL of the above suspension was dropped onto the glassy carbon electrode using a pipet gun and dried at room temperature.

Cyclic voltammograms were recorded from -0.2 to 0.8 V at scan rates of 5 mV s^{-1}. The measurements of the galvanostatic charge/discharge property and cycle-life

stability were performed with computer controlled cycling equipment (LAND CT2001A, Wuhan China). The galvanostatic charge/discharge property was measured at the current densities of 1, 2, 3, and 5 A g^{-1} with cut off voltage of 0 to 0.8 V.

3. Results and discussion

3.1. Structure and morphology characterizations

The structures of the as-prepared materials were investigated by powder X-ray diffraction (XRD) measurements. Fig. 1a shows the XRD patterns of CAC8, pure PANI and CAC8/PANI composite. For CAC8, the diffraction peaks at 2θ = 21.6° and 44.3° can be attributed to the graphite-like structure (002) and (100), respectively. The XRD pattern of pure PANI show three characteristic peaks. The peaks at 2θ of 14.9 and 25.7 resulted from the periodicity both perpendicular and parallel to the polymer chain, respectively. The peak at 2θ of 20.9 is caused by the layers of polymer chains at alternating distances [27]. The X-ray data of CAC8/PANI composite presents crystalline peaks similar to those obtained from pure PANI, meanwhile the diffraction peaks at 44.3° cannot be obvious observed, may be the CAC8 particles were interacted with PANI molecules and almost completely covered by PANI. The XRD patterns of CACs/PANI composites have similar peaks to the CAC8/PANI composite (Fig. 1b).

Typical SEM images of pure PANI, CAC8 and CACs/PANI composites are shown in Fig. 2. We can see that pure PANI particles (Fig. 2a) aggregate into lumps with diameters ranging from 100 nm to a few microns. Their surfaces are very rough because aniline polymerization is a multi-level growth process. Interestingly, as Fig.

2b illustrates, on the surface of CAC8, there are lots of hollow nanotubes forms in a highly irregular fashion with varying heights and diameters, these make the CAC8 as a support material can supply high specific surface area. Fig. 2c-g are CACs/PANI composites morphologies. They clearly indicate that CAC5/PANI is actually agglomerations of nanofibers and nanoparticles (Fig. 2c), CAC6/PANI and CAC7/PANI are netlike with intertwined nanofibers subunits structure (Fig. 2d, e). The image of CAC8/PANI has a very irregular nanocones texture with large pores, this may be occurs during the interfacial polymerization. Just like what happening in the normal interfacial polymerization, the aniline in the oil phase will diffuse into the water phase through the interface and be oxidized by the oxidant agent (APS) in the water phase to form PANI. The difference is that the aniline can also be grafted onto the CAC8 of multi-level structure to form CAC8/PANI (Fig. 2f). Similarly the CAC9/PANI shows a coral-like geometry (Fig. 2g). To obtain more detailed structural insight, the samples of the CAC8 and CAC8/PANI were investigated by TEM analysis (Fig. 3), Fig. 3a shows that CAC8 presents multi-level and hollow nanotubes structure with varying sizes. For the CAC8/PANI composite, PANI attached onto the CAC8 (Fig. 3b), which are well consistent with the SEM observation.

The BET measurements were performed to investigate the textural characteristics of CAC8 and CAC8/PANI. The N_2 adsorption-desorption isotherms are shown in Fig. 4, where the inset shows the pore size distribution of CAC8/PANI composite obtained from the analysis of N_2 desorption isotherms by using the BJH method. The BET specific surface area, pore volume and average pore size of the CAC8 and

CAC8/PANI composite are summarized in table 1. The measured BET specific surface area of CAC8 is 1568.0 m^2 g^{-1}, and C content and H content in as-prepared CAC8 are around 87.41 wt % and 0.32 wt % by combustion elemental analysis, respectively. After polymerization of PANI on the surface of CAC8, the BET specific surface area of CAC8/PANI is reduced to 145.6 m^2 g^{-1}, which indicates that the PANI was successfully attached onto the CAC8. However, as shown in the pore size distribution of the CAC8/PANI composite, there is the possibility of micropores (below 2 nm), and its pore-size distribution indicates the presence of mainly large mesopores and macropores (from 10 to 100 nm). Furthermore, this specific structure will provide the possibility of efficient electron transfer and electrolyte diffusion.

3.2. Electrochemical properties

CV is considered to be a suitable tool for estimating the difference between the non-Faradic and Faradic reactions. Fig. 5 shows CV curves obtained in a three-electrode cell for the CAC8, pure PANI and CACs/PANI composites electrodes under a scan rate of 5 mV s^{-1} in the potential window of -0.2-0.8 V . As can be seen in Fig. 5, there is no peak originating from the CAC8 electrode, which indicates the CAC8 possesses an electrical double-layer capacitance. However, the capacitance characteristic of pure PANI or CACs/PANI composites is distinct from that of the CAC8 electrode and close to the ideal rectangular shape with pseudocapacitance characteristics. Notably, under the scan rate of 5 mV s^{-1} , CAC8/PANI composite electrode has largest capacitance, which is believed to be due to the synergistic effects from each components of the composite electrode. Two pairs of well-defined redox

peaks appeared for the the CAC8/PANI composite electrode, which are attributed to two redox transitions of PANI, The first couple of peaks (about 0.21 V/0.10 V) are attributed to the redox transition of PANI between a semi-conducting state (leucoemeraldine form) and a conducting state (polaronicemeraldine form), and the second couple of peaks (about 0.48 V/0.44 V) are due to the transformation between the p-benzoquinone/hydroquinone couple because of the attack by water [28-30].

The applicability of supercapacitors can be directly evaluated by means of the galvanostatic charge-discharge method. Fig. 6 gives the curves of CAC8, pure PANI and CAC8/PANI composite electrodes at a current density of 1 A g^{-1}, and the shape of all charge/discharge curves is nearly linear and symmetric, which is characteristic of a good capacitance. The specific capacitance of the electrode can be calculated using the following equation [31-33]:

$$C_m = C / m = (I\,t) / (\Delta V\,m) \qquad (1)$$

Where C_m is specific capacitance (F g^{-1}), I is charge/discharge current (A), t is the time of discharge (s), ΔV is the voltage difference between the upper and lower potential limits, and m is the mass of the active electrode material. The specific capacitance of all the sample at the current density of 1 A g^{-1} was calculated according to Eq.(1) , the corresponding gravimetric capacitances are 207 F g^{-1} (CAC8), 251 F g^{-1} (PANI) and 597 F g^{-1} (CAC8/PANI), which indicate that the specific capacitance of the composite material (CAC8/PANI) is obviously enhanced compared with the corresponding CAC8 and pure PANI. The larger capacitance for CAC8/PANI may be caused by the combination of the electric double-layer capacitance of CAC8 and

Faradaic pseudocapacitance of PANI. During the interfacial polymerization, the carbon with multi-level structure not only serve as a highly conductive support material, but also provide a large surface for the well-dispersed deposition of nanoscale PANI particles. In addition, the loose open structure system of the CAC8/PANI composite improves the contact between the electrode and the electrolyte, thus making full use of the electrochemical active material, which is in agreement with the result of the CV curves.

Fig. 7a shows the charge/discharge curves of CAC8/PANI composite electrode at different current densities. The discharge capacitances at various current densities are plotted in Fig. 7b. The decreased capacitance of CAC8/PANI composite with the increase of discharge current densities is likely caused by the resistance of electrode and the insufficient Faradaic redox reaction of the active material under higher discharge current densities. However, the specific capacitance of the CAC8/PANI composite still retains 66% of the original value as the current density increases from 1 to 5 A g^{-1}. This result indicates the high capacitance of the CAC8/PANI composite can be maintained under high current density.

The cycling stability of the pure PANI and CAC8/PANI composite electrodes were tested at a constant current density of 1 A g^{-1} for 1000 cycles. As shown in Fig. 8, the capacitive retention of the pristine PANI quickly decreased to 60% after 400 charge/discharge cycles, however, under the same measurement conditions, the capacitive retention of CAC8/PANI is 80% after 1000 cycles. The results indicate the CAC8/PANI composite electrode has good cycling ability, which may be due to the

CAC8 (remains at about 96% of the initial capacitance after 1000 cycles) provids a robust support for the PANI, thus enhancing the mechanical strength of the composite and preventing the PANI to swelled and shrinked during the long-term cycling [34,35].

Fig. 9 represents the complex-plane electrochemical impedance spectrum (EIS) of the pure PANI and CAC8/PANI composite electrode based supercapacitor. Electrochemical impedance spectra measurements were carried out at the open-circuit potential over a frequency range of 100 kHz to 100 mHz. Each impedance spectrum has a semicircular arc and a straight line. At very high frequencies, the intercept at real part (Z') represents a combined resistance of ionic resistance of electrolyte, intrinsic resistance of substrate, contact resistance at the electrode material/current collector interface (R_e), the charge transfer resistance (R_{ct}) caused by the Faradaic reactions and the double-layer capacitance (C_{dl}) at the contact interface between electrode and electrolyte solution. The 45° slope portion of the curve is the Wurburg resistance (Z_w), which is a result of the frequency dependence of ionic diffusion/transport in the electrolyte and to the surface of the electrode [36-39]. The values of R_e for pure PANI and CAC8/PANI composite electrodes were 3.5 and 5.3 Ω, R_{ct}, which can be directly measured as the semicircular arc diameter, are 24.5 and 14.8 Ω, respectively, for pure PANI and CAC8/PANI composite. Clearly, the sum of R_e and R_{ct} of CAC8/PANI composite electrode (20.3 Ω) are smaller than pure PANI electrode (28.0 Ω), which demonstrates that the addition of CAC8 enhances conductivity and improves charge transfer performance of CAC8/PANI composite

electrode. Moreover, at low frequencies, the straight line of CAC8/PANI is nearly perpendicular to the realy axis, indicates a more facile ion diffusion process through the electrode material and it had pure capacitive behaviors [40]. Electrochemical measurements have showed that CAC8/PANI composite may be a promising candidate material for supercapacitor applications.

4. Conclusions

In conclusion, a simple synthetic strategy to prepare nanocones-structured CAC8/PANI composite via an interfacial polymerization approach. The surface morphology, structure, and capacitive behaviors of the CAC8/PANI composite test show the unique CAC8 structure provides high conductivity as well as a relatively large area on which to deposit the PANI particles, that can effectively reduce the kinetic difficulties for both charge transfer and ion transport throughout the electrode. The CAC8/PANI composite electrode exhibits excellent capacitance of 597 F g^{-1} at the current densities of 1 A g^{-1} and outstanding cycling stability above 80% of the capacitance retention after 1000 charge/discharge cycles. This facile and effective approach for the synthesis of CAC8/PANI composite has significant potential to be further exploited in supercapacitor devices.

5. Acknowledgments

We thank the Science and Technology program of Gansu Province (NO.1308RJZA295, 1308RJZA265), the National Natural Science Foundation of China (NO.21164009), the program for Changjiang Scholars and Innovative Research Team in University (IRT1177), PhD Scientific Research starting Program of Lanzhou

City University (LZCU-BS2013-11), Key Laboratory of Eco-Environment-Related Polymer Materials of Ministry of Education, and Key Laboratory of Polymer Materials of Gansu Province.

References

1 P. Simon and Y. Gogotsi, Nat Mater, 2008, **7**, 845-854.

2 J. R. Miller and A. F. Burke, Electrochemical Society Interf, 2008, **17**, 53-57.

3 T. Y. Wei, C. H. Chen, H. C. Chien, S. Y. Lu and C. C. Hu, Adv Mater, 2010, **22**, 347-351.

4 A. Burke, Electrochim Acta, 2007, **53**, 1083-1091.

5 J. R. Miller and P. Simon, Science, 2008, **321**, 651-652.

6 Y. Zhang, H. Feng, X. Wu, L. Wang, A. Zhang, T. Xia, H. Dong, X. Li and L. Zhang, Int J Hydrogen Energy, 2009, **34**, 4889-4899.

7 D. Zhang, X. Zhang, Y. Chen, P. Yu, C. Wang and Y. Ma, J Power Sources, 2011, **196**, 5990-5996.

8 S. Chen, J. Zhu, X. Wu, Q. Han and X. Wang, ACS nano, 2010, **4**, 2822-2830.

9 H. Sun, W. He, C. Zong and L. Lu, ACS Appl Mater Interfaces, 2013, **5**, 2261-2268.

10 Z. Li, L. Zhang, B. S. Amirkhiz, X. Tan, Z. Xu, H. Wang, B. C. Olsen, C. M. B. Holt and D. Mitlin, Adv Energy Mater, 2012, **2**, 431-437.

11 L. F. Chen, Z. H. Huang, H. W. Liang, Q. F. Guan and S. H. Yu, Adv Mater, 2013, **25**, 4746-4752.

12 K. Kuratani, K. Okuno, T. Iwaki, M. Kato, N. Takeichi, T. Miyuki, T. Awazub, M. Majimab and T. Sakai, J Power Sources, 2011, **196**, 10788-10790.

13 H. Wang, Z. Li, J. K. Tak, C. Holt, X. Tan, Z. Xu, B. S. Amirkhiza, D. Harfieldc, A. Anyiac, T. Stephensona and D. Mitlin, Carbon, 2013, **57**, 317-328.

14 A. Jain, V. Aravindan, S. Jayaraman, P. S. Kumar, R. Balasubramanian, S. Ramakrishna, S. Madhavi and M. P. Srinivasan, Sci. Rep, 2013, **3**, 1-6.

15 M. Yang, B. Cheng, H. Song and X. Chen, Electrochim Acta, 2010, **55**, 7021-7027.

16 K. Lota, V. Khomenko and E. Frackowiak, J Phys Chem Solids, 2004, **65**, 295-301.

17 Y. G. Wang, H. Q. Li and Y. Y. Xia, Adv Mater, 2006, **18**, 2619-2623.

18 J. Yan, T. Wei, Z. Fan, W. Qian, M. Zhang, X. Shen and F. Wei, J Power Sources, 2010, **195**, 3041-3045.

19 J. Yan, T. Wei, B. Shao, Z. Fan, W. Qian, M. Zhang and F. Wei, Carbon, 2010, **48**, 487-493.

20 M. N. Hyder, S. W. Lee, F. C. Cebeci, D. J. Schmidt, Y. ShaoHorn and P. T. Hammond, Acs Nano, 2011, **5**, 8552-8561.

21 C. XianáGuo and C. MingáLi, Energy Environ Sci, 2011, **7**, 4504-4507.

22 Z. F. Li, H. Zhang, Q. Liu, L. Sun, L. Stanciu and J. Xie, ACS Appl Mater Interfaces, 2013, **5**, 2685-2691.

23 J. H. Liu, J. W. An, Y. C. Zhou, Y. X. Ma, M. L. Li, M. Yu and S. Li, ACS Appl Mater Interfaces, 2012, **4**, 2870-2876.

24 A. K. Sarker and J. D. Hong, Langmuir, 2012, **28**, 12637-12646.

25 H. Fan, H. Wang, N. Zhao, X. L. Zhang and J. Xu, J Mater Chem, 2012, **22**, 2774-2780.

26 Y. Li, X. Zhao, Q. Xu, Q. H. Zhang and D. J. Chen, Langmuir, 2011, **27**, 6458-6463.

27 L. Li, A. R. O. Raji, H. Fei, Y. Yang, E. L. G. Samuel, and J. M. Tour, ACS Appl Mater Interfaces, 2013, **5**, 6622-6627.

28 H. Zhang, Q. Zhao, S. Zhou, N. Liu, X. Wang, J. Li and F. Wang, J Power Sources 2011, **196**, 10484-10489.

29 D. W. Wang, F. Li, J. Zhao, W. Ren, Z. G. Chen, J. Tan, Z. S. Wu, I. Gentle, G. Q. Lu and H. M. Cheng, ACS Nano, 2009, **3**, 1745-1752.

30 H. Peng, G. Ma, W. Ying, A. Wang, H. Huang, Z. Lei, J Power Sources, 2012, **211**, 40-45.

31 Z. Fan, J. Yan, L. Zhi, Q. Zhang, T. Wei, J. Feng, M. Zhang, W. Qian and F. Wei, Adv Mater, 2010, **22**, 3723-3728.

32 S. Numao, K. Judai, J. Nishijo, K. Mizuuchi and N. Nishi, Carbon, 2009, **47**, 306-312.

33 A. L. M. Reddy and S. Ramaprabhu, J Phys Chem C, 2007, **111**, 7727-7734.

34 P. C. Chen, G. Shen, Y. Shi, H. Chen and C. Zhou, ACS Nano, 2010, **4**, 4403-4411.

35 Z. Fan, J. Yan, T. Wei, L. Zhi, G. Ning, T. Li and F. Wei, Adv Funct Mater, 2011, **21**, 2366-2375.

36 Y. He, W. Chen, X. Li, Z. Zhang, J. Fu, C. Zhao and E. Xie. ACS Nano, 2013, **7**, 174-182.

37 M. D. Stoller, S. J. Park, Y. W. Zhu, J. H. An and R. S. Ruoff, Nano Lett, 2008, **8**, 3498-3502.

38 A. Di Fabio, A. Giorgi, M. Mastragostino and F. Soavi, J Electrochem Soc, 2001, **148**, A845-850.

39 P. Yang, X. Xiao, Y. Li, Y. Ding, P. Qiang, X. Tan, W. Mai, Z. Lin, W. Wu, T. Li, H. Jin, P. Liu, J. Zhou, C. P. Wong, and Z. L. Wang, ACS Nano, 2013, **7**, 2617-2626.

40 J. Chen, K. Sheng, P. Luo, C. Li and G. Shi, Adv Mater, 2012, **24**, 4569-4573.

Figure captions:

Fig. 1 (a) XRD patterns of CAC8, pure PANI and CAC8/PANI composite, (b) XRD patterns of composites CACs/PANI with various pyrolyzed temperature of chestnut shells.

Fig. 2 FE-SEM images of (a) pure PANI, (b) CAC8, (c) CAC5/PANI, (d) CAC6/PANI, (e) CAC7/PANI, (f) CAC8/PANI and (g) CAC9/PANI.

Fig. 3 TEM images of CAC8 (a) and CAC8/PANI composite (b).

Fig. 4 Nitrogen adsorption-desorption isotherms of CAC8 and CAC8/PANI composite. The inset shows the pore size distribution curve of CAC8/PANI composite.

Fig. 5 CV curves of the CAC8, pure PANI and CACs/PANI composites electrodes within the potential window -0.2-0.8 V at a scan rate of 5 mV s^{-1} in 1 M H_2SO_4.

Fig. 6 Galvanostatic charge/discharge curves of CAC8, pure PANI and CAC8/PANI composite electrodes at a current density of 1 A g^{-1} in 1 M H_2SO_4.

Fig. 7 (a) Galvanostatic charge/discharge curves of CAC8/PANI composite electrodes at various current densities in 1 M H_2SO_4. (b) the corresponding discharge capacitances.

Fig. 8 Cycling stability of pure PANI, CAC8 and CAC8/PANI at a current density of 1 A g^{-1}.

Fig. 9 Nyquist plots of pure PANI and CAC8/PANI composite in 1 M H_2SO_4. The inset shows the expanded high frequency region of the plot.

Table 1 The BET specific surface areas, average pore size, and pore volumes of

CAC8 and CAC8/PANI composite.

Fig. 1

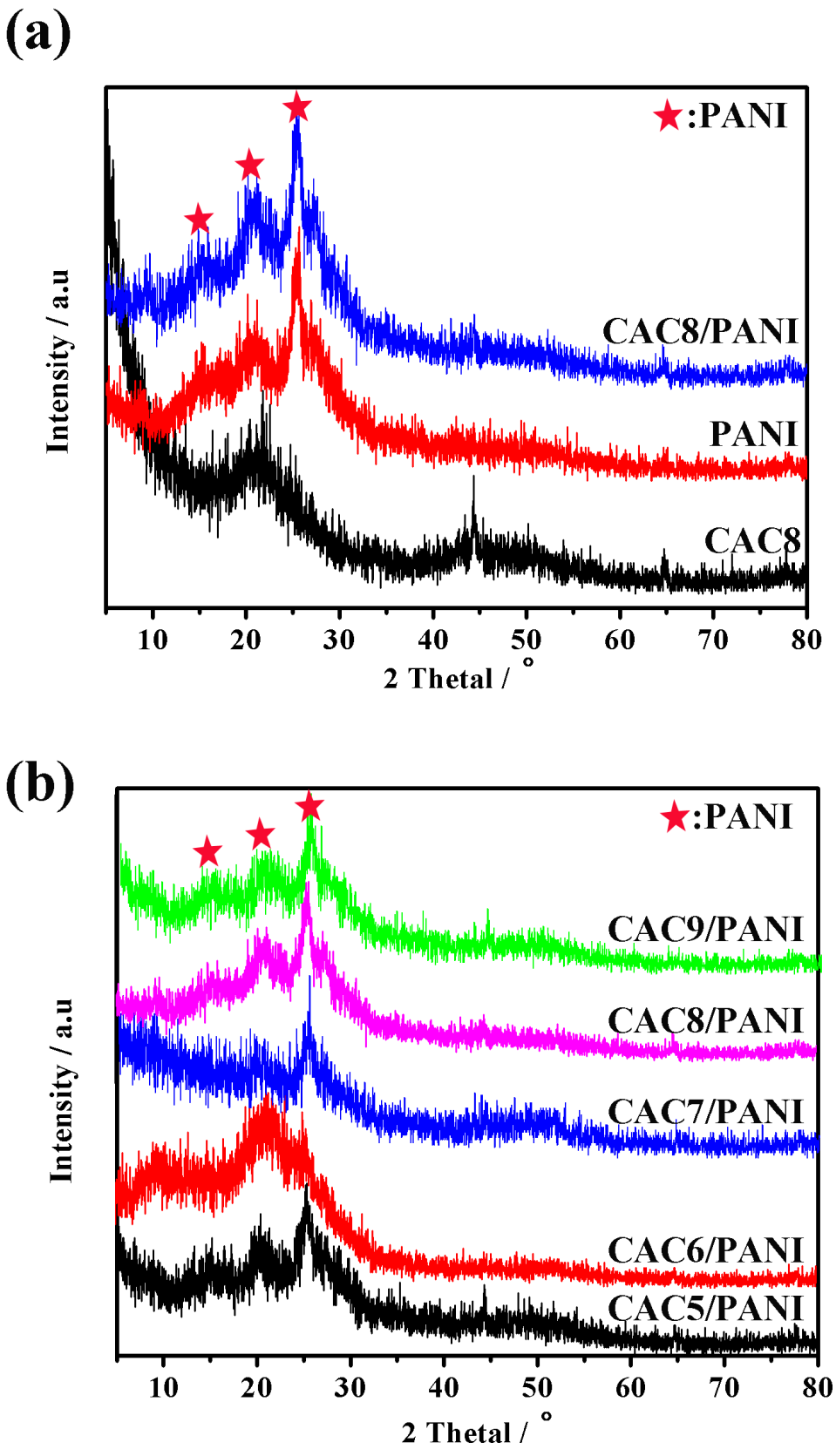

Fig. 2

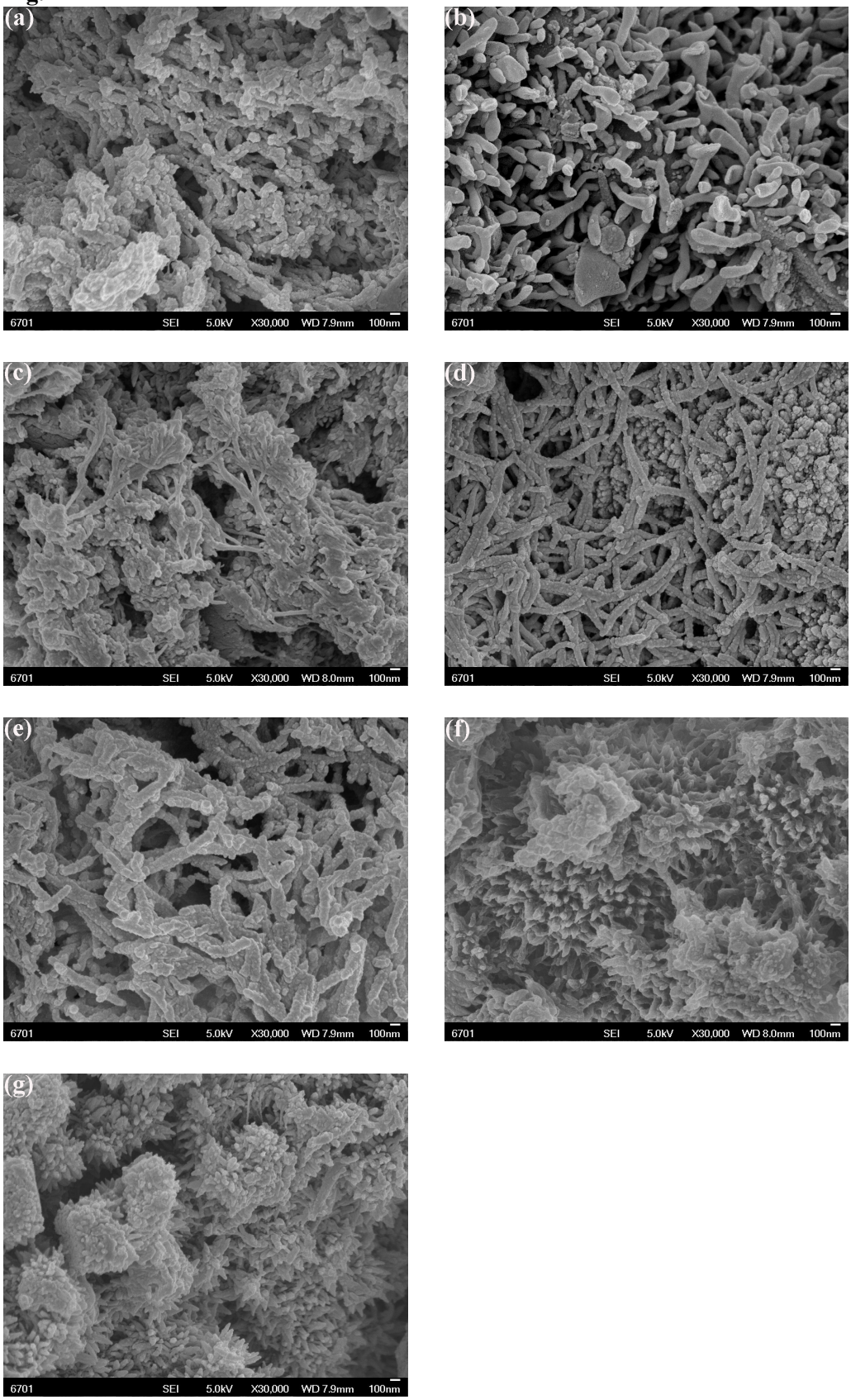

Fig. 3

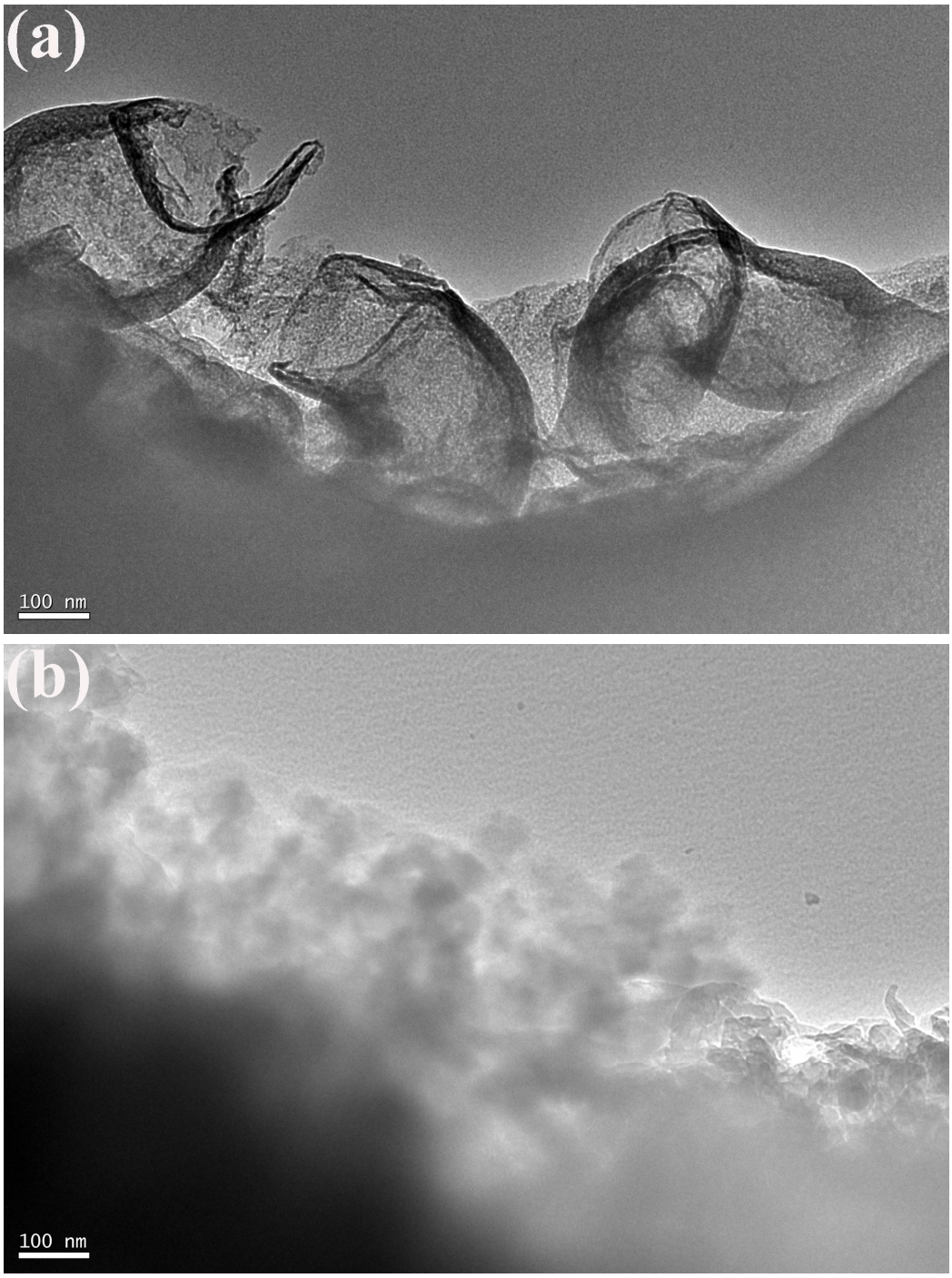

Fig. 4

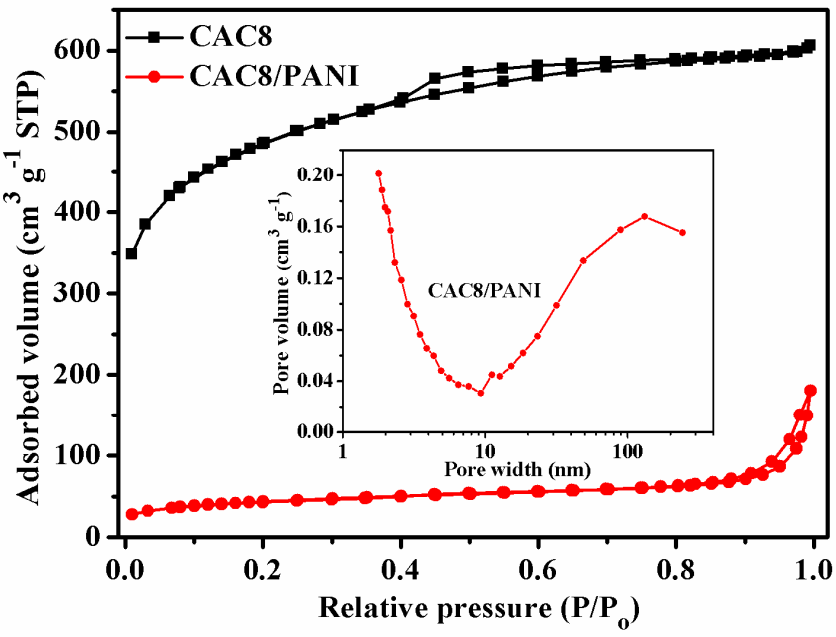

Fig. 5

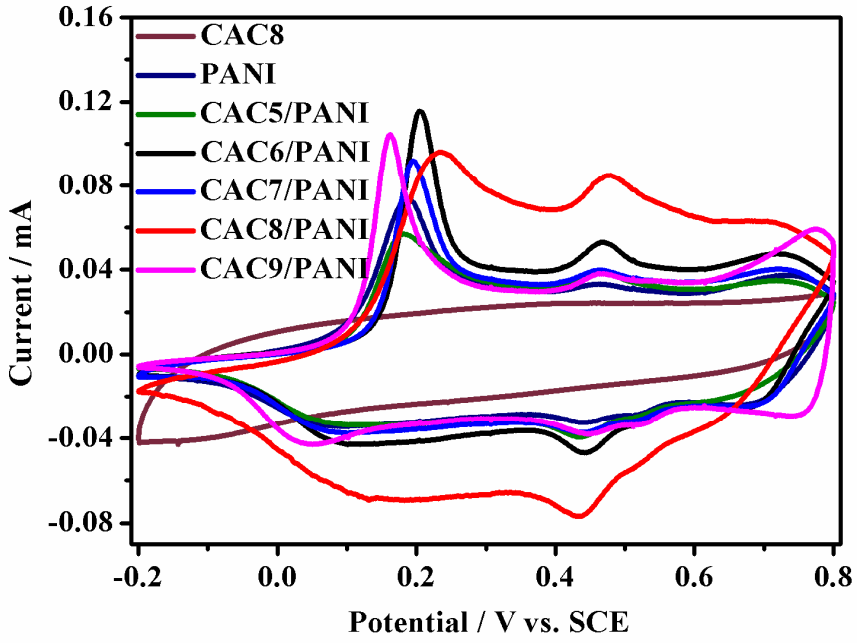

Fig. 6

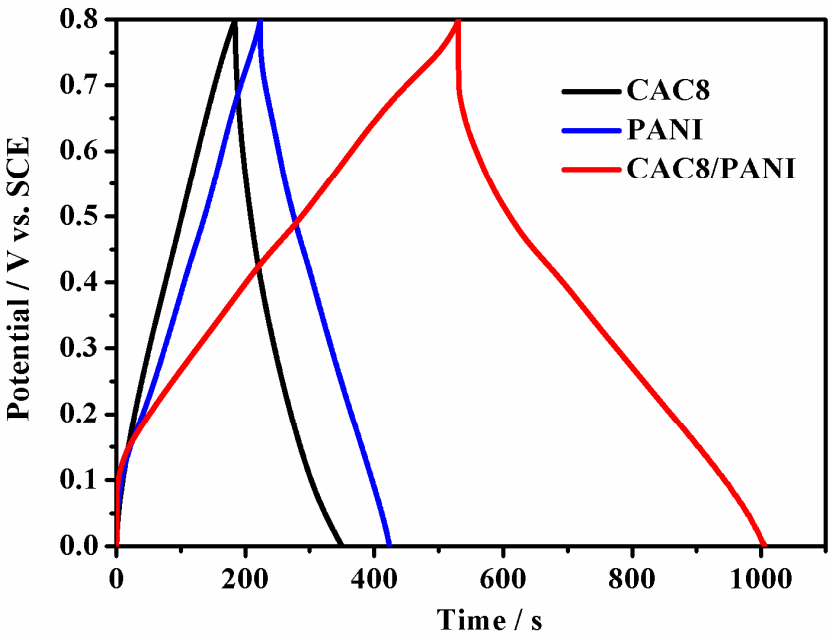

Fig. 7

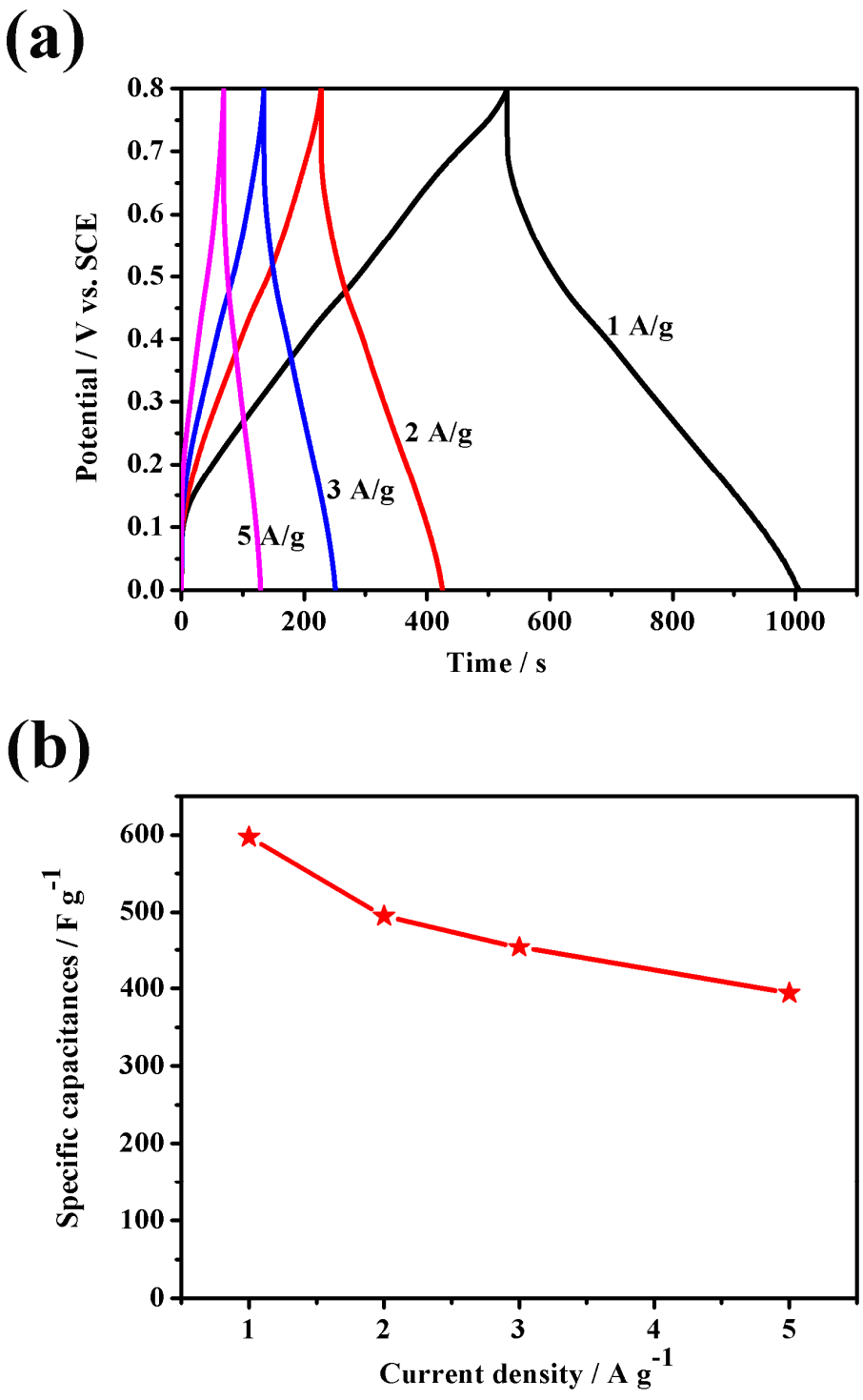

Fig. 8

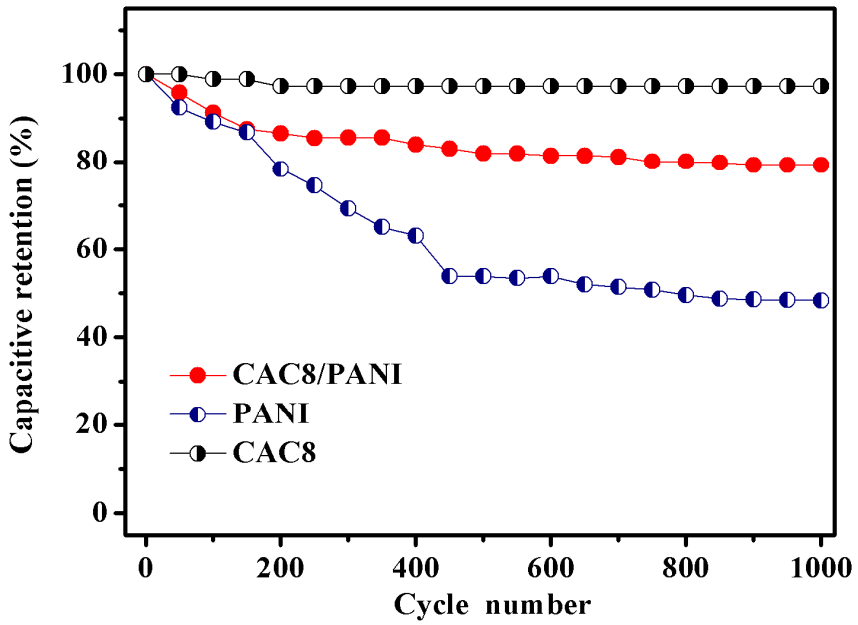

Fig. 9

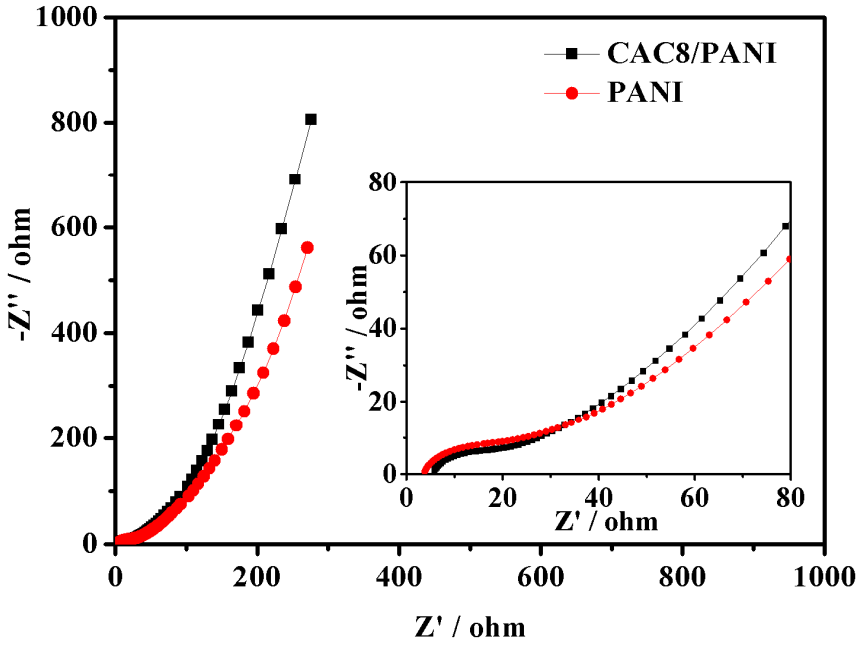

Table 1

Samples	S_{BET} (m^2 g^{-1})	*Average pore size (nm)*	*Pore volume* (cm^3 g^{-1})
CAC8	1568.0	2.4	0.94
CAC8/PANI	145.6	7.7	0.28

Table of contents

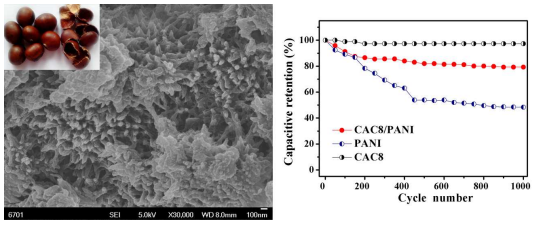

The electrochemical performance of the electrode materials can be enhanced by the synergistic effects of the polyaniline and multi-level structure bio-carbon.

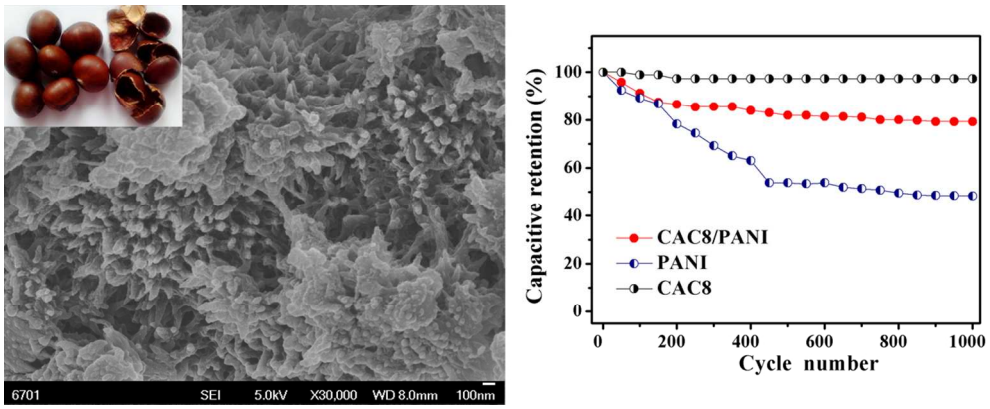

468x187mm (72 x 72 DPI)